ChemComm

Precious Metal-Free Solar-to-Fuel Generation: SSM-DSCs Powering Water Splitting with NanoCOT and NiMoZn Electrocatalysts

Journal:	*ChemComm*
Manuscript ID	CC-COM-11-2019-009209.R1
Article Type:	Communication

COMMUNICATION

Precious Metal-Free Solar-to-Fuel Generation: SSM-DSCs Powering Water Splitting with NanoCOT and NiMoZn Electrocatalysts

Received 00th January 20xx,
Accepted 00th January 20xx

DOI: 10.1039/x0xx00000x

Hammad Cheema,[a] Jonathon Watson,[a] Pravin S. Shinde,[b] Roberta R. Rodrigues,[a] Shanlin Pan,[b] and Jared H. Delcamp[a,*]

A precious metal-free sequential series multijunction dye-sensitized solar cells (SSM-DSCs)-powered water electrolysis system is demonstrated using NanoCOT and NiMoZn electrodes. A stable 3.9% solar-to-hydrogen (STH) efficiency is achieved using a recently reported black organic dye and graphene electrodes for DSCs.

Finding sustainable energy production systems is one of the most pressing challenges of the 21st century.[1, 2] Production of hydrogen (H_2) from water on large scale with the only energy input being from the sun is an attractive method for a sustainable energy future.[3, 4] While solar-to-electric energy conversion is gaining widespread utilization, systems are critically needed to mitigate the intermittent nature of sunlight.[3, 5, 6] In this regard, solar-to-fuel conversion systems are a promising solution, in that, fuels can be generated during solar irradiation hours, stored for extended time periods, and used on demand during dark hours.[2, 7] Water splitting to generate H_2 and O_2 is one of the most straightforward approaches that can address the global need for a fuel on a larger scale. Additionally, H_2 is a zero-emission fuel with a higher gravimetric heating value compared to gasoline and diesel which can be stored and transported.[4, 8] The design of systems that can power the water-splitting reaction without the use of precious metals is highly desirable.[3, 4] Two interesting strategies for solar powered water splitting are through the use of photoelectrochemical cells (PECs) and photovoltaic-electrochemical cells (PV-ECs).[4] While examples of these systems are known in the literature, none are currently economically viable on a global scale.[9, 10] The advantage of the PV-EC approach is that each component can be optimized separately for a specific role in a full system.[11] Precious metal-free PV-EC water splitting systems are urgently needed to demonstrate the use of inherently low-cost materials toward solar-to-fuel conversion. This manuscript puts forward a PV-EC system using only precious metal-free components based on abundant materials both for the photovoltaic (PV) and electrocatalyst (EC) components (Fig. 1).

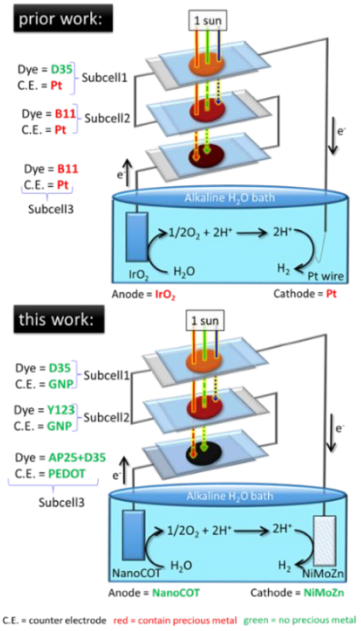

Fig. 1. Comparison of a prior SSM-DSC-EC system with key component changes shown.

A minimum thermodynamic potential energy for water splitting of –1.23 V (ΔE^o, standard reaction potential) must be supplied to allow for the cathodic ($2H^+ + 2e^- \rightarrow H_2$) and anodic ($H_2O \rightarrow 2e^- + 2H^+ + ½\ O_2$) half-reactions.[7] With catalyst overpotential requirements in mind, practically 1.9-2.0 V of overall energy is required for efficient water splitting from a photovoltaic cell since catalyst overpotentials and practical current densities (which are potential dependent) must be accounted for.[7, 12] However, sluggish kinetics of the oxygen evolution reaction (OER) and widespread use of precious metal-based catalysts (Ru, Ir, and Pt) have traditionally lowered the practicality for large scale application of a PV-EC system.[13, 14] Recently, a nanostructured carbon, oxygen and titanium-based (NanoCOT) with high efficiency for the OER as an anode was reported.[15] NanoCOT has shown impressively enhanced catalytic activity under alkaline conditions due to its nanostructured nature and dominant presence of reduced Ti states as active sites.[15] Similarly, electrocatalytic NiMoZn (nickel, molybdenum, and zinc) as

[a] 481 Coulter Hall, Chemistry Department, University of Mississippi, University, MS, 38677, USA. Email: delcamp@olemiss.edu
[b] Department of Chemistry and Biochemistry, The University of Alabama, Tuscaloosa, Alabama 35487, United States.
†Electronic supplementary information (ESI) available: Experimental details about device assembly protocols, electrolyte, and dye adsorption solution preparation. See DOI: 10.1039/x0xx00000x

a ternary alloy based on the earth-abundant metals is very promising as a cathode.[16]

With precious metal-free electrodes available as electrocatalysts, a photovoltaic system with a single illuminated area sequential series multijunction (SSM)-DSC was selected as the power source for a PV-EC system.[17, 18] DSCs are unique in terms of aesthetics, scalability, low light performance and precious metal-free material options.[19-25] The incredible performance of DSCs in low light situations makes them ideal for a multilayer construct with a single illuminated area where photon flux is filtered by the upper active layers resulting in low light conditions for the bottom active layers. In SSM-DSCs, high energy photons are used by the upper active layers to generate high photovoltages, and lower energy photons can be harvested using near-infrared (NIR) sensitizers as lower active layers.[26] In our recent report, SSM-DSCs with three subcells achieved a greater than 2.3 V output, 10.1% solar-to-electric conversion, and 6.6% solar-to-hydrogen (STH) conversion efficiency.[26] However, the application of a precious metal-based counter electrode (CE) such as Pt and ruthenium-based sensitizers in the previously reported system could lower practical applicability. To circumvent this, a precious metal-free high photovoltage output SSM-DSC system is put forward (Fig. 1). From the prior system, the ruthenium dyes have been replaced with a red organic dye **Y123** and a recently reported organic black dye **AP25** (Fig. 2 and S1, Table S1, ESI†).[17, 18, 27] The sensitizers were selected based on their complementary absorption profiles, efficient use of low light intensity, and ability to work efficiently on thinner cells with metal complex redox shuttles (Fig. S2-S3, Table S1, ESI†).[17, 18] Additionally, the Pt counter electrode has been replaced by either graphene nanoplatelets (GNP) for transparent counter electrodes or poly(3,4-ethylenedioxythiophene) (PEDOT) for the final non-transparent counter electrode.[28, 29]

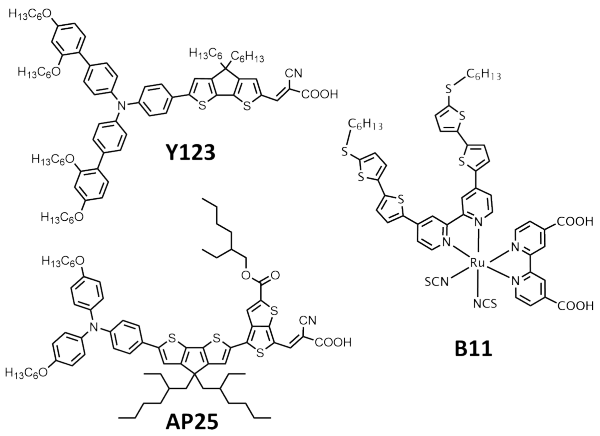

Fig. 2. Chemical structures of sensitizers **Y123**, **AP25** and **B11**.

The power conversion efficiency (PCE) of single DSCs and SSM-DSCs was calculated according to the equation PCE = ($J_{sc} \times V_{oc} \times FF$)/$I_0$ where J_{sc} is the short-circuit current density, V_{oc} is the open-circuit voltage, FF is the fill factor and I_0 is the intensity of the incident light (1 sun, air mass 1.5G). First, GNP performance was tested with organic dye **Y123** and $Co(bpy)_3^{3+/2+}$ (bpy is 2,2'-bipyridine) as the redox shuttle to optimize conditions. Device parameters were studied as a performance matrix with the best device results having minimal transmission losses were obtained by drop-casting a GNP suspension (1 mg GNP ml^{-1} isopropanol) and wiping off any excess powder after the isopropanol had evaporated (Fig. S4 and Table S2, ESI†). The individual subcells were optimized in terms of TiO_2 thickness, sensitizer absorption breadth, and redox shuttle choice (Fig. S1-S3 and S5, Tables S1 and S3, ESI†). The film thickness and sensitizer absorption profile mainly determine the photocurrent output at each subcell and the number of transmitted photons to the following subcells. Ideally, the photon flux within the SSM-DSC device should be equally divided among the subcells. Thus, the first and second subcells in the SSM-DSCs (Fig. 1) should employ the widest optical gap sensitizer (**D35**, λ_{onset} = 570 nm, λ_{max} = 500 nm)[30, 31] and the moderate optical gap sensitizer (**Y123**, λ_{onset} = 650 nm, λ_{max} = 540 nm)[32] with redox shuttles paired to generate the highest photovoltage from thinner photoanodes to allow for photon passage to the final narrow optical gap sensitizer (**AP25**, λ_{onset} = 780 nm, λ_{max} 660 = nm)[27] subcell (Table S1, ESI†).[33-36] The redox shuttle selection determines the photovoltage output and the possible peak incident photon-to-current conversion efficiency (IPCE) which changes with counter electrode selection (Fig. S3 and S6, Table S4). The top subcell with sensitizer **D35** was paired with known $Co(bpy\text{-}pz)_2^{3+/2+}$ (where bpy-pz is (6-1H-pyrazol-1-yl)-2,2'-bipyridine) as the redox shuttle for a maximum possible V_{oc} of 1.36 V.[30, 31] **D35** provides exceptional TiO_2 surface insulation to slow recombination losses to the electrolyte with a good photocurrent on relatively thin TiO_2 films.[37] An optimized thickness of 1.5 µm was adopted for the front cell (**D35**, Fig. S5, Table S3, ESI†) to give a balanced photocurrent density (5.7 mA cm^{-2}) with transmission to the lower subcells in the SSM-DSC device. For the second subcell with **Y123**, a thickness of 3 µm was selected with the $Co(bpy)_3^{3+/2+}$ redox shuttle (Fig. S5, Table S3, ESI†). Replacement of $Co(bpy\text{-}pz)_2^{3+/2+}$ with $Co(bpy)_3^{3+/2+}$ was strategically done to achieve a higher photocurrent (11.6 mA cm^{-2} compared to 9.4 mA cm^{-2}, Table S3, ESI†) for the **Y123**-based DSC device which is roughly double that of the first **D35** subcell at 5.7 mA cm^{-2}. For the final subcell, a co-sensitized **AP25+D35** device was tested both with GNP and PEDOT counter electrodes (Table S3, ESI†) with an optimized TiO_2 active layer thickness of 15 µm (18 nm particle size) and a 5 µm thick TiO_2 (>100 nm particle size) scattering layer to collect all remaining photons transmitted. An iodide/triiodide redox shuttle was used for this subcell for maximal photocurrent density. PEDOT as the counter electrode substantially outperforms a GNP based device with higher values for all metrics (PCE of 7.5% compared to 2.2%, Table S3, Fig. S5, ESI†). The IPCE spectra of the single and in the stack devices (individually) are shown in Fig. S6, and S7 (ESI†), and the integrated area values are in close agreement with the observed J_{sc} values from the *J-V* curves with a difference of less than 10%.

After optimizing the individual subcells, the full SSM-DSC device was tested (Table 1 and Fig. 3). The photocurrent density of the 2nd and 3rd subcells is lower due to filtered light as expected relative to the subcells measured outside the construct. For a series connection, the current through each subcell should be balanced for maximum PCE values. If the currents are mismatched, then the PCE will be lowered largely due to a reduction in FF observed via the IV curves. The photocurrent is well matched in the **D35**-$Co(bpy\text{-}pz)_2^{3+/2+}$/**Y123**-$Co(bpy)_3^{3+/2+}$/**AP25**+**D35**-$I^-/I_3^-$ SSM-DSC system leading to a high overall PCE of 8.5% (Table 1). See Table S4 and Fig. S8 (ESI†) for additional SSM-DSC constructs with apparent mismatched photocurrents. The generation of >5 mA cm^{-2} throughout the SSM-DSC device with a good FF (0.69) is made possible due to the very high photocurrent generating **AP25**+**D35** third subcell producing electricity until 900 nm and the use of anti-reflective coatings to reduce photon losses (Fig. S6, S7, ESI†).[26, 27, 38, 39]

Table 1. Summary of DSCs device data for **D35**, **Y123** and co-sensitized **AP25+D35** dyes.[a]

Dye (TiO_2 Thickness)/Redox shuttle	Position	V_{oc} (mV)	J_{sc} (mA cm^{-2})	FF (%)	PCE (%)
D35 (1.5 µm)/$Co(bpy\text{-}pz)_2^{3+/2+}$	front	1004 ± 5	5.7 ± 0.3	64 ± 1	3.7 ± 0.3
Y123 (3.0 µm)/$Co(bpy)_3^{3+/2+}$	itself	791 ± 20	11.6 ± 0.2	71 ± 1	6.5 ± 0.2
	2nd	788 ± 3	4.7 ± 0.1	76 ± 1	2.8 ± 0.1
AP25+**D35** (15 µm)/(I^-/I_3^-)	itself	608 ± 11	18.0 ± 0.5	70 ± 1	7.5 ± 0.1
	3rd	577 ± 20	4.9 ± 0.1	74 ± 1	2.3 ± 0.1
D35/Y123/AP25+D35	**SSM-DSC**	**2366 ± 18** (2391)	**5.1 ± 0.2** (5.3)	**69 ± 2** (67)	**8.2 ± 0.3** (8.5)

[a] Only the **AP25**+**D35** subcell employs a 5 µm thick scattering layer (>100 nm TiO_2 nanoparticles). All the devices employ an antireflective CYTOP coating. See the experimental section for device assembly details. Values are the average of 3 or more devices. Values in parenthesis for the last entry are the highest values observed. "itself" is the device when measured out of the **SSM-DSCs** configuration. The terms 2nd and 3rd refer to the subcell measured at that position in the **SSM-DSC** configuration.

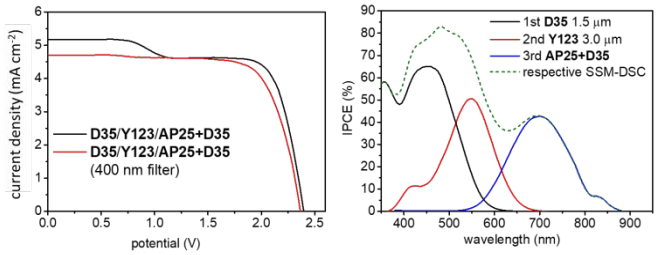

Fig. 3. Left: *J-V* curves for the optimized SSM-DSC device with and without a 400 nm filter. Right: IPCE of individual DSC devices within the SSM-DSC architecture (solid lines) and the summed spectra of the full SSM-DSC device as a dashed line.

Prior precious metal-free dyes reported in literature have typically not shown the IPCE breadth needed to generate ~5 mA cm^{-2} with <~650 nm photons being filtered by earlier subcells. The SSM-DSC shows a higher overall PCE of 8.2% (8.5% champion SSM-DSC device) compared to any individual device in the construct (maximum PCE observed from a single subcell: 7.5%). Importantly, a V_{OC} of 2.4 V is observed for this SSM-DSC device, which is high enough to power the water-splitting reaction with many electrocatalyst systems. The precious metal-free SSM-DSC device is comparable to the PCE and photovoltage from the previously highest reported precious metal-containing SSM-DSC device (PCE: 8.5% vs. 10.1% and V_{OC}: 2.4 V vs. 2.3 V, respectively).[26] Prior literature reports have shown that it is critical to block <400 nm to avoid degradation of the front Co-redox shuttle based subcell during prolonged irradiation.[17] The addition of a 400 nm filter led to a small decrease in PCE to 8.1% from 8.5% (Fig. 3, Table S5, ESI†).

A precious metal-free SSM-DSC with a maximum 2.4 V output is attractive for powering solar-to-fuel conversion.[40] The electrocatalysts selected, NanoCOT (anode) and NiMoZn (cathode), require a potential of 1.9 V to pass a current density of >2 mA cm^{-2} (Fig. 4). The SSM-DSC device is well suited to power this PV-EC system with the selected electrodes since the 1.9 V potential is near the maximum power point of the SSM-DSC device *J-V* curve. This ensures that a maximum photocurrent can flow through this system with minimal overpotential losses during water-splitting.[11]

The SSM-DSC/NanoCOT/NiMoZn PV-EC system gives a solar-to-hydrogen conversion efficiency of 3.9% according to the equation $\eta_{H_2} = (J_{op} \times E^o_{(H_2O/H_2)} \times FE)/I_o$, where J_{op} is the operating current density(3.7 mA cm^{-2}), $E^o_{(H_2O/H_2)}$ is the thermodynamic

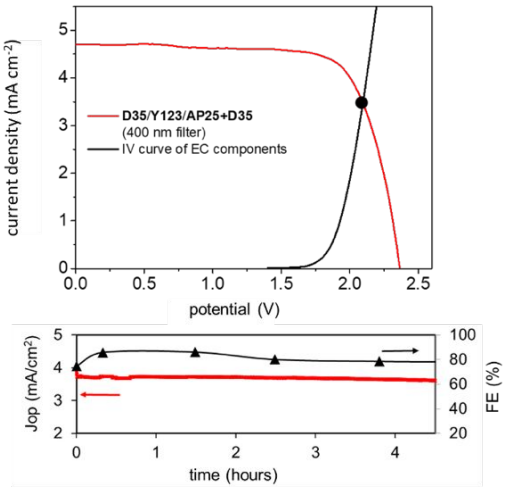

Fig. 4. PV-EC *J-V* results. The EC components were measured in a two-electrode setup in 0.1 M KOH, with a scan rate of 5 mV s^{-1} (top). The black dot highlights the operating point for a PV-EC device. J_{op} and *FE* as a function of time is shown for the PV-EC system (bottom). Results are representative of at least 3 devices.

free energy change (1.23 V for water splitting), *FE* is the faradaic efficiency (86%), and η_{H_2} is the solar-to-hydrogen conversion efficiency (Fig. 4 and Table S6, ESI†).[16] The precious metal-free PV-EC system was found to power water splitting with a stable J_{op} and η_{H_2} over the course of 5 hours (h) of continuous illumination without signs of decomposition. After 5 h, the SSM-DSC device was disconnected, and the *J-V* curve shows only modest changes (Fig. S8-S9 and Table S7, ESI†). These findings are significant given the potential for cost-effective fuel production when the raw materials for the PV-EC systems in Figure 1 are compared with solar-to-fuel efficiencies (Tables S8 & S9, ESI†).

In conclusion, by careful selection of components, a precious metal-free PV-EC system was shown to power the water-splitting reaction at 3.9% solar-to-hydrogen conversion efficiency. The PV, an SSM-DSC device, was designed for balanced transmission and absorption through strategically selected precious metal-free organic sensitizers in place of the previously reported Ru-based

sensitizers and by adjusting the TiO_2 thicknesses to control photon flux at each subcell. A solar-to-electric PCE of 8.5% with 2.4 V output was observed. GNP and PEDOT were employed successfully as replacement counter electrodes for Pt in the DSC subcell counter electrodes. The SSM-DSC gave up to a 2.4 V output and was shown to power a water-splitting system with NanoCOT/NiMoZn (anode/cathode) electrocatalysts with sustained performance for 5 hours. The entirely precious metal-free photovoltaic-electrolysis system demonstrated stable 3.9% solar-to-hydrogen efficiency. Future directions include designing SSM-DSCs with even higher photocurrents while retaining photovoltages near 2.4 V for PV-EC systems to boost the overall solar-to-hydrogen conversion efficiencies.

Conflicts of interest

There are no conflicts to declare.

Acknowledgments

All of this research, except the electrocatalyst preparation, was supported by the U.S. Department of Energy, Office of Science, Office of Basic Energy Sciences, under Award DE-SC0019131. P.S.S. and S.P. thank the National Science Foundation (NSF) for award 1539035, which supported the preparation of electrocatalyst electrodes.

Corresponding Author*

*Jared H. Delcamp, delcamp@olemiss.edu

1. J. A. Turner, *Science*, 2004, **305**, 972-974.
2. J. Turner, G. Sverdrup, M. K. Mann, P. C. Maness, B. Kroposki, M. Ghirardi, R. J. Evans and D. Blake, *Int. J. Energy Res.*, 2008, **32**, 379-407.
3. J. H. Montoya, L. C. Seitz, P. Chakthranont, A. Vojvodic, T. F. Jaramillo and J. K. Nørskov, *Nat. Mater.*, 2017, **16**, 70-81.
4. J. H. Kim, D. Hansora, P. Sharma, J.-W. Jang and J. S. Lee, *Chem. Soc. Rev.*, 2019, **48**, 1908-1971.
5. N. S. Lewis, *Science*, 2007, **315**, 798-801.
6. J. J. Concepcion, R. L. House, J. M. Papanikolas and T. J. Meyer, *Proc. Natl. Acad. Sci.*, 2012, **109**, 15560-15564.
7. M. G. Walter, E. L. Warren, J. R. McKone, S. W. Boettcher, Q. Mi, E. A. Santori and N. S. Lewis, *Chem. Rev.*, 2010, **110**, 6446-6473.
8. J. Nowotny, C. Sorrell, L. Sheppard and T. Bak, *Int. J. Hydrog. Energy*, 2005, **30**, 521-544.
9. A. M. Abdalla, S. Hossain, O. B. Nisfindy, A. T. Azad, M. Dawood and A. K. Azad, *Energy Convers. Manag.*, 2018, **165**, 602-627.
10. J. D. Holladay, J. Hu, D. L. King and Y. Wang, *Catal. Today.*, 2009, **39**, 244-260.
11. J. Jia, L. C. Seitz, J. D. Benck, Y. Huo, Y. Chen, J. W. D. Ng, T. Bilir, J. S. Harris and T. F. Jaramillo, *Nat. Commun.*, 2016, **7**, 13237.
12. T. Bak, J. Nowotny, M. Rekas and C. Sorrell, *Int. J. Hydrog. Energy*, 2002, **27**, 991-1022.
13. T. E. Rosser, M. A. Gross, Y.-H. Lai and E. Reisner, *Chem. Sci.*, 2016, **7**, 4024-4035.
14. B. Zhang and L. Sun, *Chem. Soc. Rev.*, 2019, **48**, 2216-2264.
15. Z. Shan, P. S. Archana, G. Shen, A. Gupta, M. G. Bakker and S. Pan, *J. Am. Chem. Soc.*, 2015, **137**, 11996-12005.
16. J. P. Torella, C. J. Gagliardi, J. S. Chen, D. K. Bediako, B. Colón, J. C. Way, P. A. Silver and D. G. Nocera, *Proc. Natl. Acad. Sci.*, 2015, **112**, 2337-2342.
17. H. Cheema, R. R. Rodrigues and J. H. Delcamp, *Energy Environ. Sci.*, 2017, **10**, 1764-1769.
18. R. R. Rodrigues, H. Cheema and J. H. Delcamp, *Angew. Chem.*, 2018, **57**, 5472-5476.
19. B. O'Regan and M. Grätzel, *Nature*, 1991, **353**, 737-740.
20. A. Hagfeldt, G. Boschloo, L. Sun, L. Kloo and H. Pettersson, *Chem. Rev.*, 2010, **110**, 6595-6663.
21. H.-G. Han, H. C. Weerasinghe, K. Min Kim, J. Soo Kim, Y.-B. Cheng, D. J. Jones, A. B. Holmes and T.-H. Kwon, *Sci. Rep.*, 2015, **5**, 14645.
22. A. Fakharuddin, R. Jose, T. M. Brown, F. Fabregat-Santiago and J. Bisquert, *Energy Environ. Sci.*, 2014, **7**, 3952-3981.
23. Y. Ren, D. Sun, Y. Cao, H. N. Tsao, Y. Yuan, S. M. Zakeeruddin, P. Wang and M. Grätzel, *J. Am. Chem. Soc.*, 2018, **140**, 2405-2408.
24. S. Yoon, S. Tak, J. Kim, Y. Jun, K. Kang and J. Park, *Build. Environ.*, 2011, **46**, 1899-1904.
25. S. Ahmad, E. Guillen, L. Kavan, M. Grätzel and M. K. Nazeeruddin, *Energy Environ. Sci.*, 2013, **6**, 3439-3466.
26. H. Cheema and J. H. Delcamp, *Adv. Energy Mater.*, 2019, **9**, 1900162.
27. H. Cheema, J. Watson, A. Peddapuram, and J. H. Delcamp, *Chem. Commun.*, 2019, submitted.
28. L. Kavan, J.-H. Yum and M. Grätzel, *Nano Lett.*, 2011, **11**, 5501-5506.
29. H. Ellis, N. Vlachopoulos, L. Häggman, C. Perruchot, M. Jouini, G. Boschloo and A. Hagfeldt, *Electrochim. Acta*, 2013, **107**, 45-51.
30. D. P. Hagberg, X. Jiang, E. Gabrielsson, M. Linder, T. Marinado, T. Brinck, A. Hagfeldt and L. Sun, *J. Mater. Chem.*, 2009, **19**, 7232-7238.
31. J. H. Yum, E. Baranoff, F. Kessler, T. Moehl, S. Ahmad, T. Bessho, A. Marchioro, E. Ghadiri, J. E. Moser, C. Yi, M. K. Nazeeruddin and M. Grätzel, *Nat. Commun.*, 2012, **3**, 631.
32. H. N. Tsao, C. Yi, T. Moehl, J. H. Yum, S. M. Zakeeruddin, M. K. Nazeeruddin and M. Grätzel, *ChemSusChem*, 2011, **4**, 591-594.
33. H. Cheema and J. H. Delcamp, *ACS Appl. Mater. Interfaces*, 2017, **9**, 3050-3059.
34. P. Brogdon, H. Cheema and J. H. Delcamp, *ChemSusChem*, 2018, **11**, 86-103.
35. S. H. Kang, M. J. Jeong, Y. K. Eom, I. T. Choi, S. M. Kwon, Y. Yoo, J. Kim, J. Kwon, J. H. Park and H. K. Kim, *Adv. Energy Mater.*, 2017, **7**, 1602117.
36. P. Brogdon, H. Cheema and J. H. Delcamp, *ChemSusChem*, 2017, **10**, 3624-3631.
37. S. Feldt, E. A. Gibson, E. Gabrielsson, S. Sun, G. Boschloo and A. Hagfeldt, *J. Am. Chem. Soc.*, 2010, **132**, 16714-16724.
38. T. Kinoshita, J. T. Dy, S. Uchida, T. Kubo and H. Segawa, *Nat. Photon.*, 2013, **7**, 535-539.
39. T. Yamaguchi, Y. Uchida, S. Agatsuma and H. Arakawa, *Sol. Energy Mater. Sol. Cells*, 2009, **93**, 733-736.
40. J. Luo, J. H. Im, M. T. Mayer, M. Schreier, M. K. Nazeeruddin, N. G. Park, S. D. Tilley, H. J. Fan and M. Grätzel, *Science*, 2014, **345**, 1593-1596.
41. S. R. Raga and F. Fabregat-Santiago, *Phys. Chem. Chem. Phys.*, 2013, **15**, 2328-2336.
42. W. J. Chang, K.-H. Lee, H. Ha, K. Jin, G. Kim, S.-T. Hwang, H.-m. Lee, S.-W. Ahn, W. Yoon and H. Seo, *ACS Omega*, 2017, **2**, 1009-1018.
43. A. D. Vos, *J. Phys. D*, 1980, **13**, 839-846.

TOC Graphic:

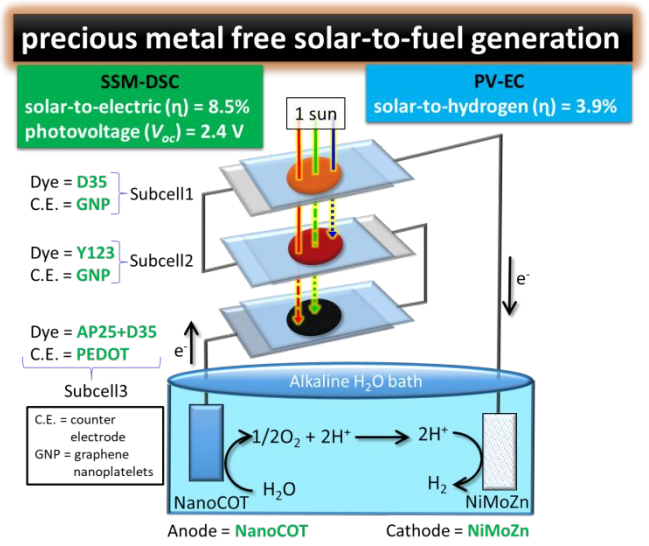
precious metal free solar-to-fuel generation
SSM-DSC
solar-to-electric (η) = 8.5%
photovoltage (V_{oc}) = 2.4 V
PV-EC
solar-to-hydrogen (η) = 3.9%
1 sun
Dye = D35
C.E. = GNP
Subcell1
Dye = Y123
C.E. = GNP
Subcell2
Dye = AP25+D35
C.E. = PEDOT
Subcell3
e-
e-
C.E. = counter electrode
GNP = graphene nanoplatelets
Alkaline H_2O bath
$1/2O_2 + 2H^+$
$2H^+$
H_2O
H_2
NanoCOT
NiMoZn
Anode = NanoCOT
Cathode = NiMoZn